

Unsteady dynamics of a classical particle-wave entity

Rahil N. Valani^{1,*}, Anja C. Slim^{2,3}, David M. Paganin¹, Tapio P. Simula⁴, and Theodore Vo²

¹*School of Physics and Astronomy, Monash University, Victoria 3800, Australia*

²*School of Mathematics, Monash University, Victoria 3800, Australia*

³*School of Earth, Atmosphere and Environment, Monash University, Victoria 3800, Australia and*

⁴*Centre for Quantum and Optical Science, Swinburne University of Technology, Melbourne 3122, Australia*

(Dated: June 1, 2025)

A droplet bouncing on the surface of a vertically vibrating liquid bath can walk horizontally, guided by the waves it generates on each impact. This results in a self-propelled classical particle-wave entity. By using a one-dimensional theoretical pilot-wave model with a generalized wave form, we investigate the dynamics of this particle-wave entity. We employ different wave forms to understand the role played by both wave oscillations and spatial wave decay in the walking dynamics. In addition to steady walking, we uncover a rich set of unsteady motions such as oscillating walking, self-trapped oscillations and irregular walking. We explore the dynamical and statistical aspects of irregular walking and connect the droplet dynamics with the Lorenz equations, the Langevin equation, and deterministic diffusion.

I. INTRODUCTION

Vertically vibrating a bath of liquid can result in the emergence of a self-propelled particle-wave entity in the form of a walking droplet on the free surface of the liquid [1–4]. The walking droplet, also known as a walker, on each bounce locally generates a slowly decaying standing wave. It then interacts with these self-generated waves on subsequent bounces to propel itself horizontally. The walker emerges for vibration amplitudes just below the Faraday instability threshold where the surface of the bath remains flat everywhere except in the vicinity of the walker; above this threshold the whole interface becomes unstable to standing Faraday waves [5]. Very close to but below the Faraday threshold, the waves created by a walker on each bounce extend far in space and decay very slowly in time. In this regime, the droplet is not only influenced by the wave it created from its most recent bounce, but also by the waves it created in the distant past, giving rise to *memory* in the system. Typically, in this high-memory regime, the droplet has been shown to mimic several peculiar features that were previously thought to be exclusive to the quantum realm. These include orbital quantisation in rotating frames [6–8] and harmonic potentials [9–11], Zeeman splitting in rotating frames [12, 13], wavelike statistical behavior in confined geometries [14–18] as well as in an open system [19] and tunneling across submerged barriers [20–22]. They have also been predicted to show anomalous two-droplet correlations [23, 24]. Recently, efforts have also been made to develop a hydrodynamic quantum field theory for the walking-droplet system [25, 26]. A detailed review of hydrodynamic quantum analogs of walking droplets has been provided by Bush [27] and Bush and Oza [28].

To model the walking droplet, many theoretical descriptions have been developed over the years. These

range from phenomenological stroboscopic models that average over the vertical periodic motion of the droplet and only capture the horizontal dynamics, to sophisticated models that resolve the vertical and horizontal dynamics and the detailed evolution of the surface waves created by the walker. A review of the different models is given by Turton *et al.* [29] and Rahman and Blackmore [30]. The latter work provides a perspective through the lens of dynamical systems theory. In experiments, a single walker or superwalker [4, 31] is typically observed to travel in a straight line at a constant speed unless it encounters obstacles or other droplets. At high memories, Bacot *et al.* [32] experimentally observed multiple states of a free walker, where in addition to rectilinear constant speed motion, the droplet was also observed to walk with oscillations in speed in the walking direction. Using a theoretical model of walkers, Hubert *et al.* [33] showed that in the very-high-memory regime, the rectilinear constant speed motion of a walker becomes unstable and the walker’s horizontal dynamics becomes bimodal where it erratically switches between phases of linear motion and diffusive motion [33]. This bimodal motion shows analogies with the run-and-tumble dynamics common in swimming micro-organisms. For example, the motion of *Escherichia coli* in a nutriment-filled medium is known to display run-and-tumble dynamics [34]. Moreover, it has been observed that artificial droplet swimmers, that are used to mimic living microswimmers, can also display bimodal gait switching triggered by the interaction between the droplet and its self-generated chemical gradients [35]. This is reminiscent of gait-switching dynamics in biological organisms such as bacteria [36, 37].

Recently, Durey *et al.* [38] also explored this high-memory regime for a walker using the stroboscopic model of Oza *et al.* [39], by confining the motion of the walker to a line. Since the steady walking is neutrally stable to lateral perturbations [39], the key aspects of the instability that destabilizes the steady walking state may be captured by investigating the droplet’s dynamics confined to one dimension [40]. They identified various regimes of

* rahil.valani@monash.edu

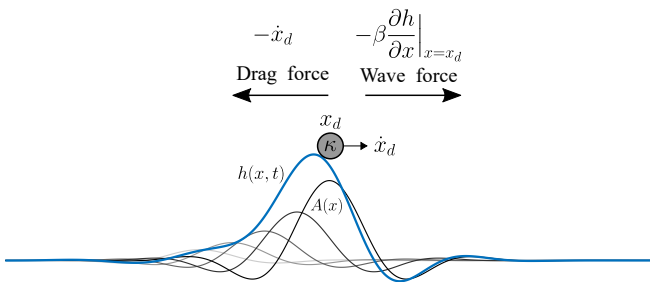


FIG. 1. Schematic of the walking droplet particle-wave system, showing a droplet of dimensionless mass κ located at x_d and walking horizontally with velocity \dot{x}_d . The droplet experiences a wave force, $-\beta \partial h / \partial x|_{x=x_d}$, from the underlying wave field $h(x, t)$ (blue curve) and a drag force, $-\dot{x}_d$. The underlying wave field $h(x, t)$ is the superposition of the individual waves (black and gray curves), of the spatial form $A(x)$ and decaying exponentially in time, that are continuously generated by the droplet along its trajectory.

a walker in the parameter space, that give rise to oscillations in the walking speed and random-walk-like motion of the droplet, leading to a statistical wavelike signature in the probability density function of the droplet's position. Wavelike statistics emerging for the speed oscillations of the walker have also been demonstrated in a hydrodynamic analog of Friedel oscillations [19].

In this paper, we revisit the dynamics of a single walker restricted to move in one horizontal dimension, by extending the stroboscopic model of Oza *et al.* [39] to a generalized wave form, i.e. allowing a general spatial structure for the underlying waves generated by the droplet, and exploring the dynamics observed in the parameter space using different wave forms. We investigate the role played by spatial decay of the wave form and wave oscillations in the droplet's dynamics by employing a Gaussian and a sinusoidal wave form respectively, and explore in detail the unsteady dynamics arising from a sinusoidal wave form. In Sec. II we present the generalized stroboscopic model and use it to perform a linear stability analysis for both the stationary state and the steady walking state of the droplet, in Secs. III and IV respectively. We then in Sec. V explore the various unsteady behaviors observed in the parameter space using different wave forms. In Secs. VI and VII we explore, respectively, the dynamical and the statistical aspects of the irregular walking motion realized in the unsteady walking regime and draw connections with the Lorenz equations, the Langevin equation and deterministic diffusion.

II. STROBOSCOPIC MODEL WITH A GENERALIZED WAVE FORM

Oza *et al.* [39] derived a stroboscopic model to describe the horizontal dynamics of a walking droplet by averaging over its vertical periodic bouncing motion and considering a Bessel function of the first kind and zeroth order,

$J_0(\cdot)$, wave form for the individual waves generated by the droplet on each bounce. Here we extend this model to an arbitrary wave form and investigate the droplet's dynamics by restricting the horizontal motion of the droplet to one dimension.

As shown schematically in Fig. 1, consider a droplet at position x_d walking horizontally with velocity \dot{x}_d and continuously generating waves with prescribed spatial structure $A(x)$ that decay exponentially in time. The equation of motion governing the horizontal dynamics of the droplet is given by,

$$\kappa \ddot{x}_d + \dot{x}_d = -\beta \frac{\partial h}{\partial x} \Big|_{x=x_d}.$$

The left hand side of this equation comprises an inertial term $\kappa \ddot{x}_d$ and a drag term \dot{x}_d , where the overdot denotes differentiation with respect to time t . The right hand side of the equation captures the forcing on the droplet by the underlying wave field $h(x, t)$. This force is proportional to the gradient of the underlying wave field. The shape of the wave field $h(x, t)$ is calculated through integration of the individual wave forms $A(x)$ that are continuously generated by the particle along its trajectory. This gives,

$$h(x, t) = \int_{-\infty}^t A(x - x_d(s)) e^{-(t-s)} ds.$$

Combining these two equations we obtain the integro-differential equation,

$$\kappa \ddot{x}_d + \dot{x}_d = \beta \int_{-\infty}^t f(x_d(t) - x_d(s)) e^{-(t-s)} ds, \quad (1)$$

where $f(x) = -A'(x)$ is the negative gradient of the wave form and the prime denotes differentiation with respect to x . The two parameters in this dimensionless equation of motion, $\kappa > 0$ and $\beta > 0$, may be usefully interpreted as the ratio of inertia to drag and the ratio of wave forcing to drag respectively.

III. THE STATIONARY SOLUTION AND ITS LINEAR STABILITY ANALYSIS

We start by seeking stationary solutions of Eq. (1). Substituting $x_d(t) = x_0$ in Eq. (1) we arrive at the condition

$$f(0) = -A'(0) = 0. \quad (2)$$

Hence, if this condition is satisfied by the wave form then we have a stationary solution.

To determine the stability of this stationary solution, we apply a perturbation $x_d(t) = x_0 + \epsilon x_1(t)H(t)$ to the stationary solution. Here $H(\cdot)$ is the Heaviside step function introduced to apply the perturbation for $t \geq 0$. Substituting this in Eq. (1), we find that the perturbation, x_1 , evolves according to

$$\kappa \ddot{x}_1 + \dot{x}_1 = \beta f'(0) \left[x_1(t) - \int_0^\infty x_1(t-z) H(t-z) e^{-z} dz \right]. \quad (3)$$

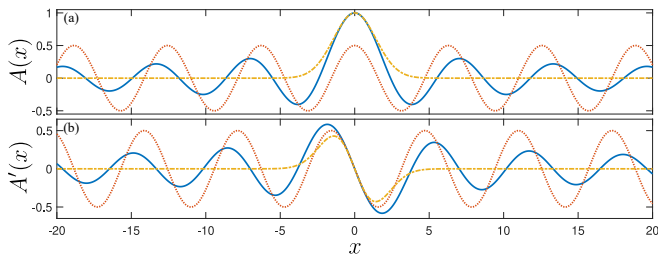


FIG. 2. Comparison of the three different wave forms $A(x)$ (a) and their gradients (b) considered in this paper: a Gaussian wave form $e^{-(x/2)^2}$ (yellow dash-dotted curve), a Bessel function wave form $J_0(x)$ (blue solid curve), and a sinusoidal wave form $\cos(x)/2$ (red dotted curve).

Taking the Laplace transform of both sides results in

$$X_1(s) = \frac{(s+1)(\kappa[sx_1(0) + \dot{x}_1(0)] + x_1(0))}{s[\kappa s^2 + (1+\kappa)s + 1 - \beta f'(0)]}. \quad (4)$$

Here $X_1(s) = \mathcal{L}\{x_1(t)\}$ with $\mathcal{L}\{\cdot\}$ denoting the Laplace transform from the time domain t to the (complex) frequency domain s . The stability of the stationary state can be determined by finding the poles of $X_1(s)$ in Eq. (4) [39]. In our case, the poles are the roots of

$$s[\kappa s^2 + (1+\kappa)s + 1 - \beta f'(0)] = 0. \quad (5)$$

The trivial $s = 0$ solution corresponds to translation invariance of the system. The non-trivial poles

$$s = \frac{-(1+\kappa) \pm \sqrt{(1+\kappa)^2 - 4\kappa(1 - \beta f'(0))}}{2}, \quad (6)$$

are both negative on a large open subset of the positive quadrant of the (κ, β) -plane. The stationary state becomes unstable when one of the poles changes sign. This takes place when

$$\beta = \frac{1}{f'(0)}. \quad (7)$$

IV. THE STEADY WALKING SOLUTION AND ITS LINEAR STABILITY ANALYSIS

Once the stationary state becomes unstable for $\beta > 1/f'(0)$, one obtains a steady walking state. We look for a steady walking solution with speed u of the generalized stroboscopic model by substituting $x_d(t) = ut$ in Eq. (1), which results in

$$u = \beta \int_0^\infty f(uz) e^{-z} dz. \quad (8)$$

By making a change of variables $uz = r$ in the integral, we can rewrite this as

$$u^2 = \beta \int_0^\infty f(r) e^{-r/u} dr = \beta F\left(\frac{1}{u}\right), \quad (9)$$

where $F(s)$ is the Laplace transform of $f(r)$. Provided that a solution to the above equation exists, one obtains the steady walking speed u of the droplet for a given parameter β and spatial wave form $A(x)$ or equivalently its gradient function $f(x)$.

To determine the stability of the steady walking solution in this generalized framework, we apply a perturbation of the form $x_d(t) = ut + \epsilon x_1(t)H(t)$ to the steady walking solution with speed u . By substituting this in Eq. (1) and comparing the $O(\epsilon)$ terms, we get

$$\kappa \ddot{x}_1 + \dot{x}_1 = \beta \left[x_1(t) \int_0^\infty f'(uz) e^{-z} dz - \int_0^\infty f'(uz) x_1(t-z) H(t-z) e^{-z} dz \right]. \quad (10)$$

Integrating the first integral term on the right side by parts gives

$$\begin{aligned} \int_0^\infty f'(uz) e^{-z} dz &= -\frac{f(0)}{u} + \frac{1}{u} \int_0^\infty f(uz) e^{-z} dz \\ &= -\frac{f(0)}{u} + \frac{1}{\beta}, \end{aligned}$$

where the constraint in Eq. (8) has been used. Substituting this in Eq. (10) and Laplace transforming, we have

$$X_1(s) = \frac{\kappa[sx_1(0) + \dot{x}_1(0)] + x_1(0)}{\kappa s^2 + s - 1 + \beta[f(0)/u + G(s)]}, \quad (11)$$

where

$$\begin{aligned} G(s) &= \mathcal{L}\{f'(ut)e^{-t}\} \\ &= \frac{1}{u} \left[-f(0) + \frac{s+1}{u} F\left(\frac{s+1}{u}\right) \right]. \end{aligned}$$

Thus,

$$X_1(s) = \frac{\kappa[sx_1(0) + \dot{x}_1(0)] + x_1(0)}{\kappa s^2 + s - 1 + (s+1) [F((s+1)/u)/F(1/u)]}. \quad (12)$$

As before, the stability of the inline walking motion can be determined by finding the poles of $X_1(s)$ in Eq. (12) [39].

To model the walking dynamics of the droplet, a Bessel function wave form, $A(x) = J_0(x)$, is typically used and has been studied in detail [38, 39]. This Bessel wave field has two key features: (i) a spatial decay and (ii) spatial oscillations. We decouple these features by considering two alternate wave forms: a Gaussian wave form $A(x) = e^{-(x/2)^2}$, which has spatial decay but no oscillations, and a sinusoidal wave form $A(x) = \cos(x)/2$, which has oscillations but no spatial decay. Both of these wave fields have been chosen such that the first and second derivatives of the wave form, $f(x)$ and $f'(x)$, match with the Bessel function wave form at the location where the wave is created. A comparison of the three wave forms and their gradients is shown in Fig. 2. We investigate the linear stability of steady walking using a Gaussian

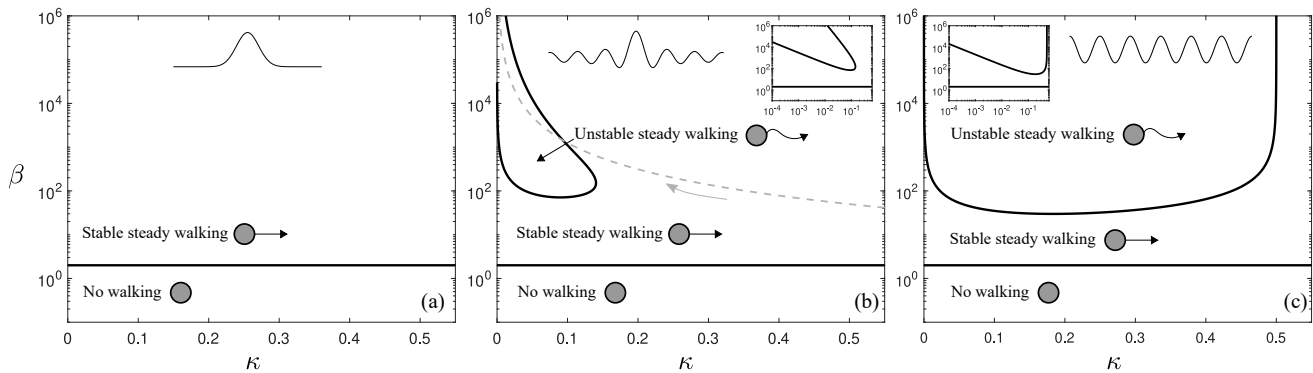


FIG. 3. Linear stability in the (κ, β) parameter space for inline perturbations to the steady walking solution of a single droplet using (a) a Gaussian wave form $e^{-(x/2)^2}$, (b) a Bessel wave form $J_0(x)$ and (c) a sinusoidal wave form $\cos(x)/2$. The gray dashed curve in panel (b) shows the path traversed in the parameter space for typical experimental parameters as the driving acceleration (or the memory) is increased. In each of panels (b) and (c), the inset shows the instability boundary using a logarithmic scale in both horizontal and vertical directions.

wave form in Sec. IV A, a Bessel wave form in Sec. IV B, and a sinusoidal wave form in Sec. IV C. To understand the effects of spatial decay and spatial oscillations on this instability, we also consider in Sec. IV D a combined sinusoidal Gaussian wave form $A(x) = \frac{1}{2} \cos(x)e^{-(x/2l)^2}$ and study the instability as the parameter l is varied.

A. A Gaussian wave form

Choosing a Gaussian wave form, $A(x) = e^{-(x/2)^2}$, results in $f(x) = (x/2)e^{-(x/2)^2}$ in Eq. (1). The corresponding equation for steady walking speed u can be obtained from Eq. (9) with

$$F\left(\frac{1}{u}\right) = 1 - \frac{\sqrt{\pi}e^{1/u^2}\text{erfc}(1/u)}{u}.$$

In the limit of large β , the speed scales as $u \sim \sqrt{\beta}$.

On performing the linear stability analysis by numerically solving for the poles of $X_1(s)$ in Eq. (12), we find that the steady walking solution always remains stable. Hence we only obtain two qualitatively different behaviors when a Gaussian wave field is considered (see Fig. 3(a)): (i) No walking for $\beta \leq 1/f'(0) = 2$ and (ii) steady walking for $\beta > 2$.

B. A Bessel wave form

Choosing a Bessel function wave form, $A(x) = J_0(x)$, results in $f(x) = -A'(x) = J_1(x)$. Hence,

$$F\left(\frac{1}{u}\right) = \frac{u^2}{1 + u^2 + \sqrt{1 + u^2}}.$$

Substituting this in Eq. (9) for the steady walking speed, we obtain

$$u = \frac{1}{\sqrt{2}} \sqrt{-1 + 2\beta - \sqrt{1 + 4\beta}}.$$

For $\beta \leq 1/f'(0) = 2$, the stationary droplet solution is stable, while for $\beta > 1/f'(0) = 2$ the steady walking solution is realized. For $\beta \gg 1$, the above equation for the walking speed can be approximated by $u \approx \sqrt{\beta}$.

The linear stability analysis requires solving for the poles of $X_1(s)$ in Eq. (12). This results in solving the equation

$$(\kappa s^2 + s - 1)\sqrt{u^2 + (s+1)^2} \left(s + 1 + \sqrt{u^2 + (s+1)^2} \right) + \beta(s+1) = 0. \quad (13)$$

For small κ and large β , a complex conjugate pair of poles cross the imaginary axis, i.e., pass through $\text{Re}(s) = 0$, resulting in a change in the stability of the steady walking solution. We can find the stability boundary of the steady walking solution in the (κ, β) parameter space by setting $\text{Re}(s) = 0$ and substituting $s = i\omega$ in Eq. (13). The linear stability diagram is shown in Fig. 3(b). We see that a lobe-shaped region appears for small κ and large β , where steady walking is unstable. For a fixed $\kappa \lesssim 0.14$, as β is increased, we get steady walking for small β , unsteady walking for moderately large β and intriguingly, we recover the steady walking state for very large β . In typical experiments with walkers and superwalkers, as the driving acceleration amplitude (or equivalently the memory) is increased, the path traversed in the (κ, β) parameter space is shown by a gray dashed curve in Fig. 3(b).

C. A sinusoidal wave form

Choosing a sinusoidal wave form, $A(x) = \cos(x)/2$, results in $f(x) = \sin(x)/2$ and we get

$$F\left(\frac{1}{u}\right) = \frac{u^2}{2(1 + u^2)}.$$

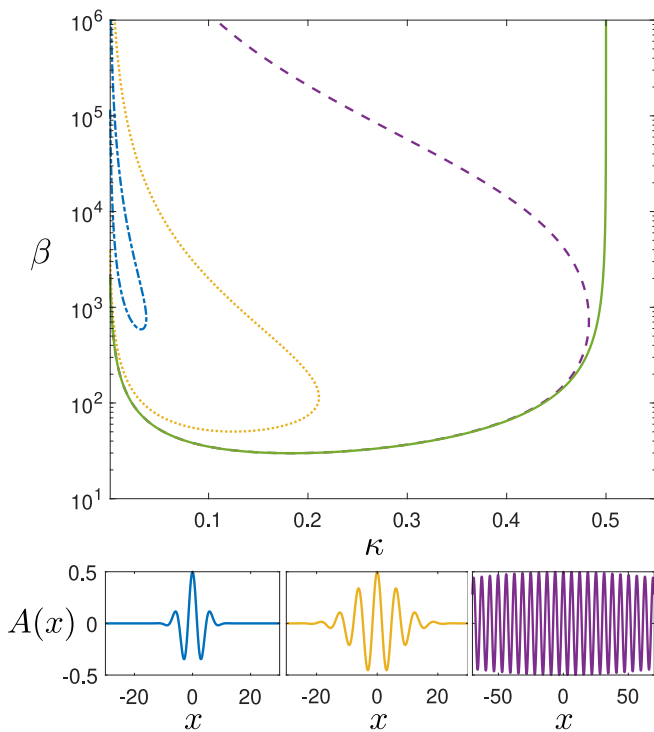


FIG. 4. Instability boundary of the steady walking solution in the (κ, β) parameter space for a wave form $A(x) = \cos(x) e^{-(x/2l)^2}/2$. Instability boundary (top panel) and the corresponding wave forms (bottom panel) are shown for $l = 2.5$ (blue dash-dotted curve), $l = 5$ (yellow dotted curve), $l = 100$ (purple dashed curve), and $l \rightarrow \infty$ (green solid curve, wave form not shown).

Thus, the steady walking speed, as determined by Eq. (9), is

$$u = \sqrt{\frac{\beta}{2} - 1}.$$

The linear stability analysis requires solving for the poles of $X_1(s)$ in Eq. (12), which results in the equation

$$(\kappa s^2 + s - 1)(2s^2 + 4s + \beta) + \beta(s + 1) = 0. \quad (14)$$

Similar to the Bessel wave form in Sec. IV B, we can find the stability boundary of the steady walking solution by setting $\text{Re}(s) = 0$ and substituting $s = i\omega$ in Eq. (14). This gives

$$\beta = \frac{2(1 + 4\kappa)}{\kappa(1 - 2\kappa)} \quad (15)$$

as the instability boundary in the parameter space (see Fig. 3(c)) with an oscillation frequency of

$$\omega^2 = \frac{\beta - 2}{2\kappa + 1} \quad (16)$$

at the onset of instability.

D. A Sinusoidal wave form with a Gaussian envelope

To further understand the effect of spatial decay of the wave form on the structure of the instability boundary, we consider a wave form $A(x) = \cos(x) e^{-(x/2l)^2}/2$ and investigate how the instability boundary in the (κ, β) parameter space is changed as the decay length scale l is varied.

Figure 4 shows the instability boundary for the steady walking state for various values of l along with the wave forms. We find that for large l , the spatial decay is very small and it does not have a significant effect on the lower boundary of the instability. However, we do see a qualitative change in the upper boundary. For a pure sinusoidal wave form that has no spatial decay, we find that the steady walking solution is always unstable for a small range of κ values as $\beta \rightarrow \infty$. For a wave form with a small but non-zero spatial decay, we recover stability of the steady walking state for large β . Conversely, for small l , we find that the region of instability shrinks rapidly with an increase in the spatial decay, indicating that oscillations in the wave form are necessary for the steady walking state to become unstable.

Thus, by homotoping from the sinusoidal wave form to an exponentially decaying sinusoid with strong decay, we have demonstrated that the oscillations in the wave form are the key dynamic mechanism responsible for the instability of the steady walker. These oscillations play important roles in the unsteady walker regime enclosed by the lobe-shaped instability boundary (Fig. 4), as we will show in the next section.

V. UNSTEADY WALKING DYNAMICS IN THE (κ, β) PARAMETER-SPACE

Once the steady walking state becomes unstable in the (κ, β) parameter space, a variety of unsteady motions are realized. We explore the resulting unsteady dynamics in the parameter space for the Bessel and the sinusoidal wave forms.

A. Bessel wave form

We have explored the unsteady dynamics of a walker by numerically integrating Eq. (1) with the Bessel wave form in the (κ, β) parameter space and the results are presented in Fig. 5. The simulations were initialized with the droplet in the steady walking state for $t < 0$. We refer the reader to Appendix A for details of the numerical implementation. On comparing the linear stability curve with the onset of instability from numerical simulations, we find a reasonably good match expect for small κ where the steady walking state becomes unstable in simulations for smaller β values compared to the linear stability prediction. This may be attributed to the bifurcation being

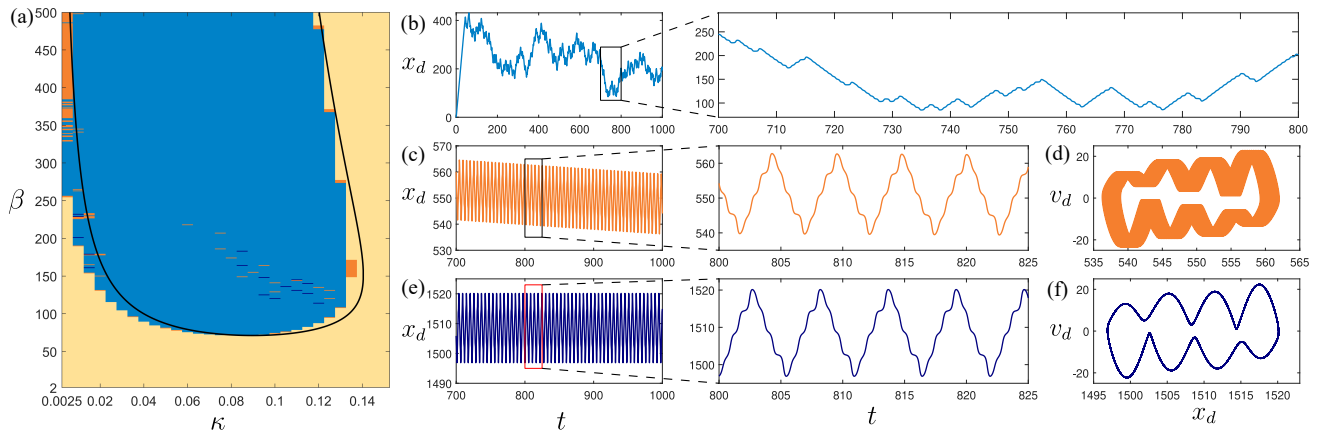


FIG. 5. Walking behaviors for a Bessel wave form. (a) Different dynamical behaviors observed in the (κ, β) parameter space at $t = 1000$ from simulations initiated at $t = 0$ with the droplet in the steady walking state for $t \leq 0$. We explore the parameter space region $0.005 \leq \kappa \leq 0.15$ and $0 < \beta \leq 500$ with resolution $\Delta\kappa = 0.005$ and $\Delta\beta = 1$. We observe steady walking (beige), oscillating walking (orange), self-trapped oscillations (navy blue) and irregular walking (blue). The solid black curve is the linear stability curve separating the steady walking and the unsteady walking regime. Typical trajectories of (b) irregular walking ($\kappa = 0.10$, $\beta = 101$), (c) oscillating walking ($\kappa = 0.12$, $\beta = 135$), and (e) self-trapped oscillations ($\kappa = 0.13$, $\beta = 128$) are shown along with the phase-space plots for (d) oscillating walking and (f) self-trapped oscillations.

a subcritical Hopf bifurcation as shown by Durey *et al.* [38].

We identify three distinct unsteady walking regimes from simulations. These are (i) irregular walkers, (ii) oscillating walkers, and (iii) self-trapped oscillations. The first of these predominates. A typical trajectory of an irregular walker is shown in Fig. 5(b). Here, the droplet performs oscillations while walking and switches the walking direction erratically. In small, isolated regions of the parameter space, we observe oscillating walkers and self-trapped oscillations. In the oscillating walker state, the droplet drifts in one direction while undergoing oscillations in the walking direction (see Fig. 5(c)). These are reminiscent of the experimentally observed velocity oscillations of a walker at high memory by Bacot *et al.* [32]. In the self-trapped oscillation state, the droplet traps itself under its self-generated wave field and performs periodic back-and-forth motion with no net drift (see Fig. 5(e)). The phase space dynamics for self-trapped oscillations shows a closed loop due to the periodic nature of the oscillations, while for oscillating walkers, we see a drift of the closed loop (see Figs. 5(f) and (d)). We note that such self-trapped periodic oscillations were also observed by Durey [41] using their one-dimensional discrete-time pilot-wave model. Moreover, self-trapped states have also been observed when the walker is free to move in two horizontal dimensions. Here, the walker's self-generated wave field confines itself to a circular orbit [11, 42, 43].

B. Sinusoidal wave form

By simulating in the (κ, β) parameter space using the sinusoidal wave form (see Appendix B for details of the numerical implementation), we observe different

unsteady regimes as shown in Fig. 6. The three distinct unsteady behaviors identified in simulations with the Bessel wave form are also realized with the sinusoidal wave form, however, the region spanned by each of those behaviors changes significantly. The oscillating walkers and the self-trapped-oscillation states occupy a significantly larger region in the parameter space compared to the small isolated regions identified using the Bessel wave form. This is due to the absence of spatial decay in the sinusoidal wave field compared to the Bessel wave field, which enhances interference of the waves. We find two distinct types of self-trapped oscillations in the parameter space. Inside the unsteady lobe region for large κ and large β , or very small κ , the self-trapped oscillations form a simple closed loop in the phase space, as shown in Fig. 6(g). In the other narrow self-trapped oscillation region, we find a dumbbell-shaped closed loop in the phase space as shown in Fig. 6(e).

Since the equation of motion with a sinusoidal wave form is simpler than with the Bessel wave form, we explore the chaotic and statistical aspects of irregular walking mainly using the sinusoidal wave field in Secs. VI and VII respectively.

VI. DYNAMICS IN THE IRREGULAR WALKING REGIME

In the irregular walking regime of the (κ, β) parameter space, we observe that the position-time trajectory of the droplet resembles a random-walk-like motion for both the Bessel and the sinusoidal wave form. To explore this in more detail, we investigate the velocity time series of the droplet undergoing irregular walking. The velocity time series, the phase space dynamics in (v_d, \dot{v}_d) space

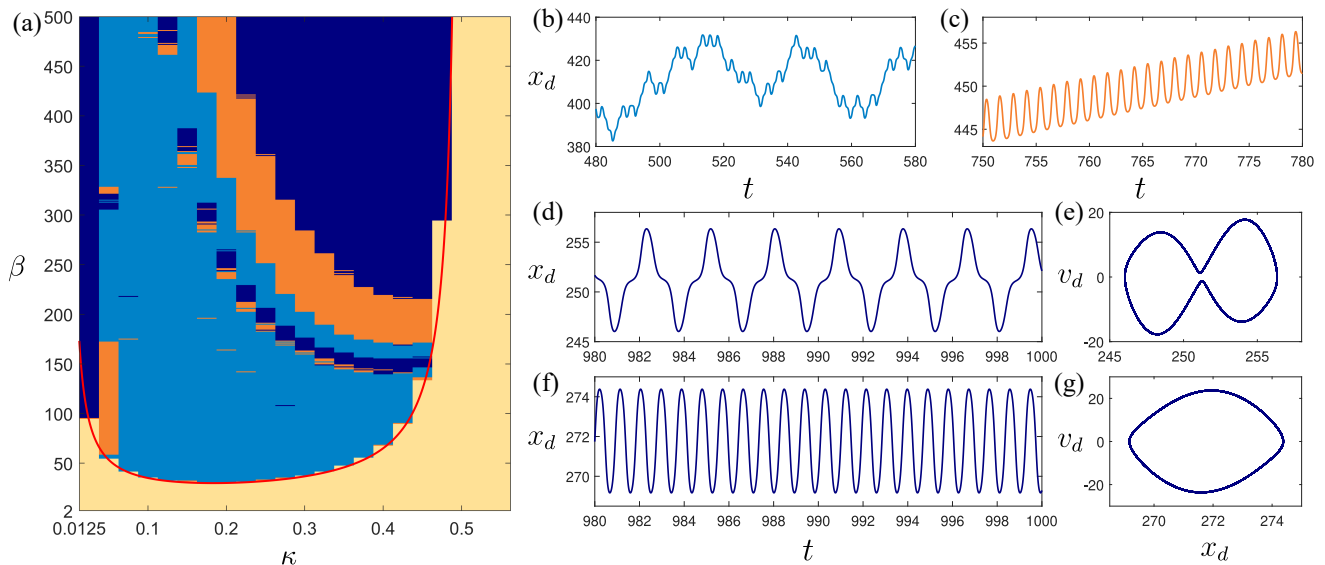


FIG. 6. Walking behaviors for a sinusoidal wave form. (a) Different dynamical behaviors observed in the (κ, β) parameter space at $t = 1000$ from simulations initiated at $t = 0$ with the droplet in the steady walking state for $t \leq 0$. We explore the parameter space region $0.025 \leq \kappa \leq 0.55$ and $0 < \beta \leq 500$ with resolution $\Delta\kappa = 0.025$ and $\Delta\beta = 1$. We observe steady walking (beige), oscillating walking (orange), self-trapped oscillations (navy blue) and irregular walking (blue). The solid red curve is the linear stability curve separating the steady walking and the unsteady walking regime. Typical trajectories of (b) irregular walking ($\kappa = 0.30, \beta = 71$), (c) oscillating walking ($\kappa = 0.30, \beta = 221$), and two different kinds of self-trapped oscillations (d) ($\kappa = 0.30, \beta = 171$) and (f) ($\kappa = 0.30, \beta = 401$) are shown. Phase space trajectories of self-trapped oscillations in (d) and (f) are shown in (e) and (g) respectively.

and the 1D return map of the maxima of the absolute velocity for typical parameter values for a sinusoidal wave form and a Bessel wave form are shown in Figs. 7(a) and (b) respectively. The velocity time series has two distinct features: (i) oscillations that correspond to speed oscillations in the walking direction and (ii) flip-flop behavior that corresponds to the reversal of the walking direction. The projection of the dynamics into the (v_d, \dot{v}_d) phase plane reveals the underlying chaotic attractor. A plot of the maximum speed $|v_{n+1}|$ on oscillation $n+1$ versus the maximum speed $|v_n|$ on the previous oscillation n generates a cusp map [44].

To understand how the droplet's dynamics change in the parameter space, we have explored the velocity time series using a sinusoidal wave form as a function of the parameter β , by fixing κ . Figure 8(a) shows the velocity bifurcation diagram where the maxima and minima v_n in the velocity time series are plotted against the parameter β , revealing regions of periodic and chaotic dynamics. Figure 8(b)-(e) shows the velocity time series and the 1D map of consecutive speed maxima at different β values. At low β , near the onset of the unsteady regime, we find that this map has a single cusp-like structure. At large β , we see multiple cusps emerging in the map. Interspersed between the chaotic regimes are periodic regimes where the 1D map collapses to a compact region. For $\beta \gtrsim 330$, the droplet transitions from the chaotic regime to the oscillating-walker regime and remain in the oscillating-walker state till $\beta = 500$.

The structures of the chaotic attractor and the cusp map for the sinusoidal wave form in Fig. 7(b) have striking resemblance to the attractor and the 1D return map of the Lorenz system [45]. Inspired by these similarities, we explore the connection between the two systems in the next section.

A. Connection to the Lorenz system

One of the classic systems that exhibits chaotic behavior is the celebrated Lorenz system [46] defined as follows:

$$\begin{aligned} \frac{dX}{dt} &= \sigma(Y - X), \\ \frac{dY}{dt} &= -XZ + rX - Y, \\ \frac{dZ}{dt} &= XY - bZ. \end{aligned} \quad (17)$$

This system has three fixed points: (i) $X = Y = Z = 0$ (unstable), (ii) $X = Y = \sqrt{b(r-1)}$ and $Z = r-1$ (stable), and (iii) $X = Y = -\sqrt{b(r-1)}$ and $Z = r-1$ (stable) for $1 < r < r_c$ with $r_c = \sigma(\sigma + b + 3)/(\sigma - b - 1)$. When $r > r_c$, all fixed points are unstable and the system exhibits either periodic or chaotic behaviour on a strange attractor [45].

Intriguingly, Takeyama [47] showed that the system of Lorenz equations in (17) can be recast into an integro-differential equation for the variable X . By eliminating

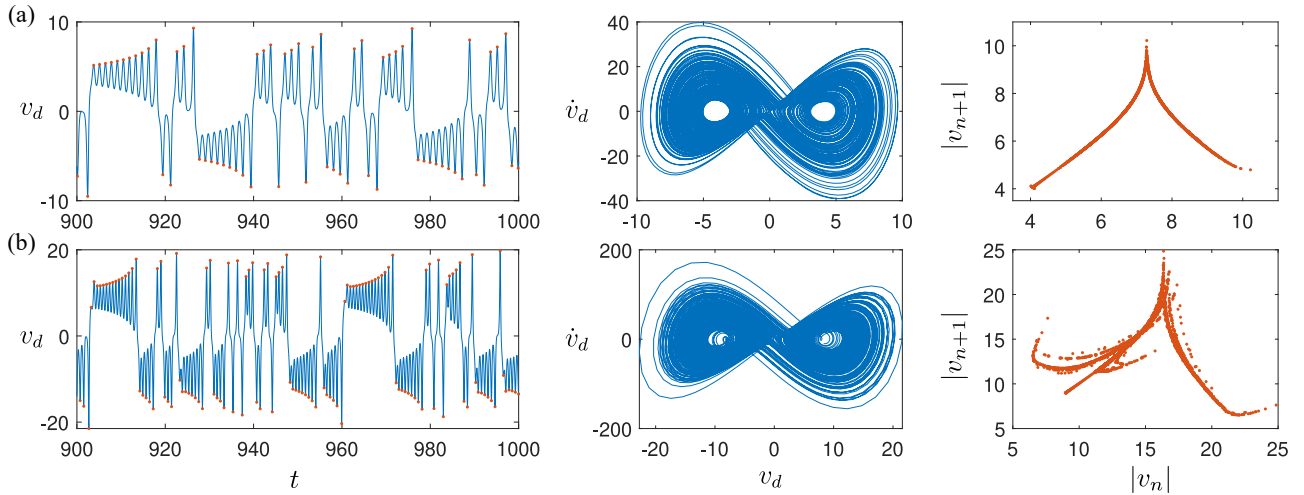


FIG. 7. Comparison of the chaotic behavior in the droplet's dynamics using (a) a sinusoidal wave field ($\kappa = 0.2$, $\beta = 35$) and (b) a Bessel wave field ($\kappa = 0.1$, $\beta = 90$). For the droplet's dynamics, the time series of velocity v_d is shown in the left panel, the projection of the chaotic attractor in the (v_d, \dot{v}_d) phase space in the middle panel and the 1D return map for the maximum speed in each oscillation in the right panel.

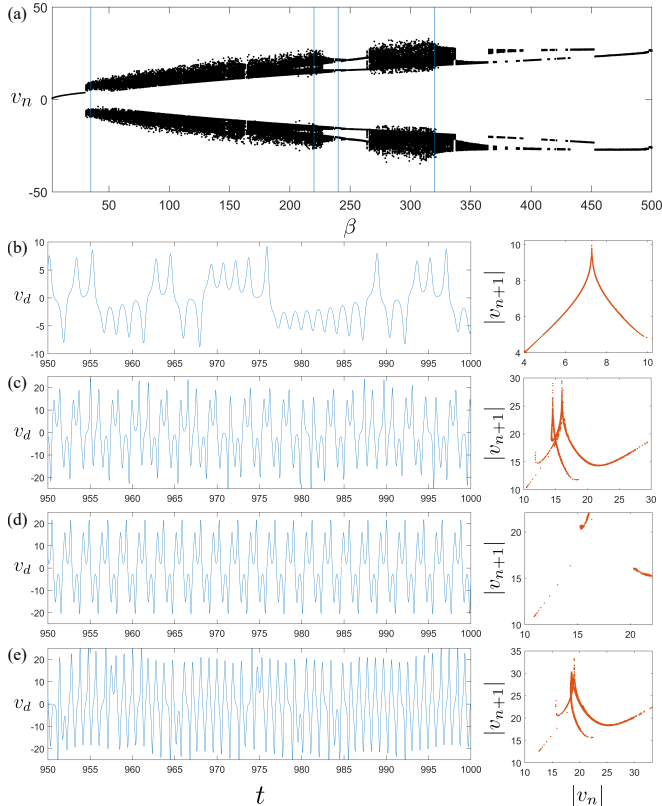


FIG. 8. (a) Velocity bifurcation diagram for the sinusoidal wave form showing the maxima and minima v_n of the velocity time series as a function of the parameter β and a fixed $\kappa = 0.2$. The time series of velocity and the corresponding map for the maximum consecutive absolute values are shown for (b) $\beta = 35$, (c) $\beta = 220$, (d) $\beta = 240$, and (e) $\beta = 320$.

the variable Y in the system of ordinary differential equations (ODEs) in Eq. (17), we get

$$\ddot{X} + (1 + \sigma)X + \sigma(1 - r + Z)X = 0, \quad (18)$$

$$\dot{Z} + bZ = X(X + \dot{X}/\sigma). \quad (19)$$

We can further eliminate Z by solving Eq. (19) for $Z(t)$ and then substituting the solution into Eq. (18). This results in the integro-differential equation

$$\ddot{X} + (1 + \sigma)\dot{X} + \sigma X \left[1 - r + \frac{1}{2\sigma} X^2 + \left(1 - \frac{b}{2\sigma} \right) \int_0^\infty X^2(t-z) e^{-bz} dz \right] = 0. \quad (20)$$

In this equation, we have dropped the terms due to the initial values that decay exponentially in time and assumed that the motion started at an infinite time in the past [47, 48]. If we assume that $b \gg 1$ and approximate the exponential term e^{-bz} in the integral of Eq. (20) by a delta function $\delta(bz)$, then the equation reduces to

$$\ddot{X} + (1 + \sigma)\dot{X} + \frac{dU}{dX} = 0,$$

with

$$U(X) = \sigma \left(\frac{1-r}{2} X^2 + \frac{1}{4b} X^4 \right).$$

This equation can be interpreted as one-dimensional motion of a particle with unit mass in a quartic potential well $U(X)$ with friction coefficient $1 + \sigma$ [47, 49]. For $r > 1$, the quartic potential well takes the form of a double-well potential with stable fixed points at $X = \pm\sqrt{b(r-1)}$ and an unstable fixed point at $X = 0$. The general expression in Eq. (20) can be rewritten by

splitting the e^{-bz} terms into a delta function and the deviation from it, giving

$$\begin{aligned} \ddot{X} + (1 + \sigma)\dot{X} + \frac{dU}{dX} \\ + \left(\sigma - \frac{b}{2}\right) X \int_0^\infty (X^2(t-z) - X^2(t)) e^{-bz} dz = 0. \end{aligned} \quad (21)$$

The above equation can be interpreted as a particle of unit mass and a friction coefficient $1 + \sigma$ in a potential well $U(X)$ with an additional force that depends on the history of the motion. Without the memory term, the particle would stop in one of the minima of the double-well potential $U(x)$, due to the damping force $-(1 + \sigma)\dot{X}$. The memory forcing sustains the particle's motion. The particle oscillates in one of the minima with growing amplitude until it has sufficient energy to cross the barrier at $X = 0$ [48, 50].

Since the velocity of the droplet in the irregular walking regime has a chaotic attractor and a cusp map similar to the Lorenz system, let us rewrite the integro-differential equation describing the motion of the droplet in Eq. (1) in terms of the velocity variable as

$$\kappa\dot{v}_d + v_d = \beta \int_{-\infty}^t f(x_d(t) - x_d(s)) e^{-(t-s)} ds. \quad (22)$$

By differentiating this equation with respect to time, we obtain the integro-differential equation

$$\kappa\ddot{v}_d + (1 + \kappa)\dot{v}_d + v_d = \beta (f(0) + v_d M(t)), \quad (23)$$

for the velocity of the droplet, where the memory forcing term is given by

$$M(t) = \int_{-\infty}^t f'(x_d(t) - x_d(s)) e^{-(t-s)} ds.$$

From the stationary solution, we know that $f(0) = 0$. Hence, differentiating the above memory term with respect to time, we get

$$\dot{M}(t) = f'(0) + v_d \int_{-\infty}^t f''(x_d(t) - x_d(s)) e^{-(t-s)} ds - M(t).$$

For the sinusoidal wave field, $f'(0) = 1/2$ and $f''(x_d(t) - x_d(s)) = -f(x_d(t) - x_d(s))$. Using this in combination with Eq. (22) we arrive at,

$$\begin{aligned} \int_{-\infty}^t f''(x_d(t) - x_d(s)) e^{-(t-s)} ds \\ = - \int_{-\infty}^t f(x_d(t) - x_d(s)) e^{-(t-s)} ds \\ = -\frac{1}{\beta}(\kappa\dot{v}_d + v_d). \end{aligned}$$

Hence, we get

$$\dot{M}(t) + M(t) = \frac{1}{2} - \frac{v_d}{\beta}(\kappa\dot{v}_d + v_d).$$

Solving this ODE for $M(t)$ gives

$$\begin{aligned} M(t) &= \int_{-\infty}^t \left(\frac{1}{2} - \frac{v_d}{\beta}(\kappa\dot{v}_d + v_d) \right) e^{-(t-s)} ds \\ &= \frac{1}{2} - \frac{\kappa}{2\beta} v_d^2 + \frac{\kappa - 2}{2\beta} \int_{-\infty}^t v_d^2(s) e^{-(t-s)} ds. \end{aligned}$$

Finally, substituting this into Eq. (23), we get

$$\begin{aligned} \ddot{v}_d + \left(1 + \frac{1}{\kappa}\right) \dot{v}_d \\ + \frac{v_d}{\kappa} \left[1 - \frac{\beta}{2} + \frac{\kappa}{2} v_d^2 + \frac{2 - \kappa}{2} \int_0^\infty v_d^2(t-z) e^{-z} dz \right] = 0. \end{aligned} \quad (24)$$

By comparing Eqs. (20) and (24), we find an exact correspondence, with the parameters in the droplet system related to the Lorenz system via

$$b = 1, r = \frac{\beta}{2} \text{ and } \sigma = \frac{1}{\kappa}.$$

Hence, using a sinusoidal wave form in the walker system, the droplet's velocity $v_d(t)$ is equivalent to the variable $X(t)$ in the Lorenz system. Thus, similarly to the interpretation of the variable X in the Lorenz system, one may interpret the velocity variable v_d in the above droplet's integro-differential equation as the position of a fictitious particle of unit mass and a friction coefficient $1 + 1/\kappa$ in a double-well potential $U(v_d)$, with an additional force that depends on the history of the motion. Conversely, one may also interpret the variable X in the Lorenz system as the velocity of a droplet of mass $1/\sigma$ which is subject to a drag force $-X$ and propelled by the memory force from the underlying sinusoidal wave that the droplet generates continuously.

We have shown the precise sequence of transformations that map the droplet dynamics to those of the Lorenz system in the case of a sinusoidal wave form. As such, our droplet dynamics immediately inherit the rich array of features that the Lorenz system possesses, including but not limited to chaotic dynamics, invariant manifold theorems, and bifurcations. The invariant manifolds of the Lorenz system are notoriously difficult to compute but can be used to understand the chaotic dynamics. For instance, it has been shown that the 2D stable manifold of the fixed point at the origin is a phase space separatrix, with all trajectories (including those on the butterfly wings) sandwiched between the sheets of this manifold [51, 52]. Supported by the results of our simulations, we expect that these invariant manifolds and the roles they play in organising the phase space, will persist when the oscillations in the wave form are modulated, as in the Bessel wave form.

We also refer the interested reader to the recent work of Durey [53], who used the properties of the Lorenz equations as a guide to explore the bifurcations and chaos in the droplet's dynamics, using an equation that is equivalent to Eq. (22).

B. Switching dynamics of irregular walking

We further explore the 1D cusp-like map to understand its relation to the droplet's dynamics. As shown in Figs. 9(a) and (b), we find that the ascending branch on the cusp map corresponds to maxima in speed oscillations when the droplet is moving in a given direction (black empty circles) while the descending branch corresponds to the maxima in speed oscillations when a flip occurs in the velocity time series or equivalently a reversal in the walking direction (red filled circles).

To analyze this further, we only look at the maximum absolute velocity after a flip occurs with a fixed number N of oscillations between the consecutive flips and plot these consecutive values against each other (see Figs. 9(c) and (d)). This map of consecutive values results in a band-like structure similar to the Continued Fraction map, also known as the Gauss map [54]. We find that in this map, each band corresponds to a fixed number N of oscillations between consecutive direction reversals. The branches corresponding to $N = 0$ (red), $N = 1$ (yellow) and $N = 2$ (purple) are shown.

VII. STATISTICAL ASPECTS OF IRREGULAR WALKING

We now turn to explore the statistical properties of the random-walk-like dynamics observed in the irregular walking regime with a sinusoidal wave form.

A. Statistical properties of irregular switching of walking direction

Aizawa [55] analyzed the statistical aspects of the Lorenz system by decomposing the time series for the system into a flip-flop process and sinusoidal oscillations with increasing amplitude (see Fig. 10(a)). We take a similar approach for the droplet's velocity time series and focus on the statistical aspects of the flip-flop process that dictates reversals in the walking direction.

The flip-flop process can also be thought of as the switches between the two attracting basins of the chaotic attractor shown in the middle panel of Figs. 7(a) and (b). Denoting the left and right attracting basins by L and R respectively, the dynamics of the flip-flop process will generate a sequence of states $LLRRLR...$ for each trajectory (see Figs. 10(b) and (c)). The probability of being found in each state, L or R , is given by $\Pr(L) = \Pr(R) = 1/2$, due to the symmetry of the system. We investigate the statistics of the flip-flop process and compare it to a Markovian process. For a Markovian flip-flop process, the transition probabilities are constant and hence calling p the probability of flipping or reversing the walking direction, we have $\Pr(L|R) = \Pr(R|L) = p$, while the probability of maintaining the walking direction is given by $\Pr(L|L) = \Pr(R|R) = 1 - p$ [56].

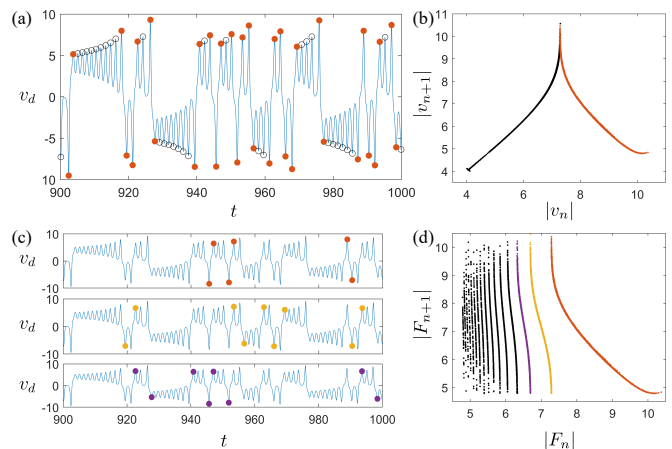


FIG. 9. Switching dynamics in the irregular walking regime for the sinusoidal wave form at $\kappa = 0.2$ and $\beta = 35$. (a) The velocity time series along with circles at the extrema of the oscillations are shown. The red filled circles indicate the extreme values of velocity before and after the flip. (b) Return map of absolute value of consecutive extrema in the time series, i.e. the absolute value of the consecutive circles in the left panel. The red and black branch corresponds to the red and black circles in the time series. (c) The same time series as in (a) but the markers now highlight the extreme values after a flip with a fixed number of N oscillations between them. The $N = 0$ (red circles), $N = 1$ (yellow circles), and $N = 2$ (purple circles) are shown. (d) The map showing consecutive absolute values of the extrema after a flip with the $N = 0$, $N = 1$, and $N = 2$ branch highlighted.

For a sequence $LLRRLRRLR...$, one can generate a chain $NJJJNJJJJ...$, where J denotes an occurrence of a jump or a walking direction reversal and N denotes that no jump has occurred. If the process is Markovian, then the probability that the phase-space trajectory will execute m turns after entering a basin before it jumps out of the basin is given by the distribution [55, 56]

$$\Pr(m) = p(1-p)^{m-1}. \quad (25)$$

Similarly, for a Markovian process, the probability that J jumps have occurred in a sequence of M turns is given by [55, 56]

$$\Pr(J|M) = \binom{M}{J} p^J (1-p)^{M-J}. \quad (26)$$

We can estimate these probabilities from sufficiently long chains of the flip-flop process for the walker from simulations by using

$$\Pr(m) = \frac{\sum_{k=1}^N \delta_{m,i_k}}{N} \quad \text{and} \quad \Pr(J|M) = \frac{\sum_{k=1}^T \delta_{J,J_k}}{T}. \quad (27)$$

Here δ is the Kronecker delta, i_k represents the number of turns executed in the basin between the $k-1$ st and k th jump, N is the total number of jumps in the sample and J_k is the number of jumps occurring in each of the T sequences of M turns of the k th subdivided sample.

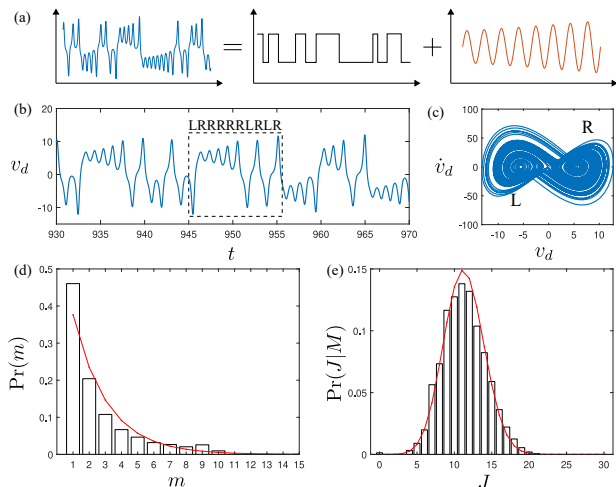


FIG. 10. Statistics of the flip-flop process for $\kappa = 0.2$ and $\beta = 65$ using the sinusoidal wave field. (a) Schematic showing that a typical velocity time-series $v(t)$ of the droplet in the random walk-like regime can be thought of as a sum of a flip-flop process $J(t)$ and an exponentially increasing sinusoidal $S(t)$ which dictates the flip after the amplitude reaches some threshold value [55]. (b) Time series of velocity for a typical droplet's trajectory in the random walk-like regime and (c) the corresponding projection of the chaotic attractor. The attractor has two basins that are labeled left 'L' and right 'R'. Panel (d) shows the probability distribution for having m oscillations between flips, while panel (e) shows the probability distribution for the number of jumps J in a given sequence of M steps. In both panels (d) and (e), the histogram is from the numerical simulations while the red curves are best fits obtained using Eqs. (25) and (26) respectively.

Figures 10(d) and (e) shows the comparison of these probability distributions calculated from an ensemble average of 100 trajectories in the simulations (histograms) and the corresponding best fits of Eqs. (25) and (26) for a typical κ and β value in the irregular walking regime. For the parameters chosen in Fig. 10, we obtain $p = 0.376$. We find a good fit at these parameters suggesting that the Markovian approximation is reasonable in certain regions of the parameter space. However, we note that this Markovian approximation does not give a good fit in the entire irregular walking regime of the parameter space. This is also true for the Lorenz system where the Markovian approximation gives a good fit in some regions of parameter space while in other regions there are sharp deviations from the Markovian process [56].

B. Connection with the Langevin equation

We also compare the equation of motion of the droplet in Eq. (1), with a Langevin-type equation that describes the motion of a particle under stochastic forcing [57],

$$\dot{q} + \gamma q = \xi(t). \quad (28)$$

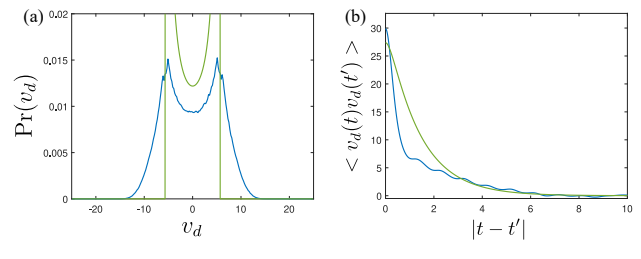


FIG. 11. Stationary probability distribution and autocorrelation for the velocity flip-flop process at $\kappa = 0.2$ and $\beta = 65$ using the sinusoidal wave field. Panel (a) shows the stationary probability distribution for velocity while panel (b) shows the plot of velocity autocorrelation function. In both panels, the blue curve is from numerical simulations of a walker while the green curve is the fit obtained by using the Langevin model with dichotomous noise.

Here q is the dynamical variable, γ is the friction coefficient and $\xi(t)$ is the stochastic forcing. Comparing this equation with the droplet's equation of motion for a sinusoidal wave field,

$$\dot{v}_d + \frac{1}{\kappa} v_d = \frac{\beta}{\kappa} \int_0^\infty \frac{1}{2} \sin(x_d(t) - x_d(t-z)) e^{-z} dz, \quad (29)$$

we see that the dynamical variable q is equivalent to the velocity v_d of the droplet, the friction coefficient γ is equivalent to $1/\kappa$ and the stochastic forcing in Eq. (28) takes the place of the memory forcing in Eq. (29). The wave force on the walker in the irregular walking regime has a time series similar to the velocity time series where the oscillating force switches erratically between positive and negative values. We can crudely approximate the memory-force time series for the droplet as a flip-flop process and ignore the oscillations. Then, the force time series of the droplet resembles a dichotomous process where the values of the force flip randomly between only two possible values. If we choose the stochastic noise $\xi(t)$ in Eq. (28) to be a dichotomous process, then we can compare the Langevin dynamics with the numerical simulations of the droplet's dynamics. We assume that $\xi(t)$ is a dichotomous process that will have only two possible values $\pm\Delta$ with equal probability and jumps between them at a rate $\lambda/2$ [57]. This form of the forcing has zero mean and autocorrelation

$$\langle \xi(t)\xi(t') \rangle = \Delta^2 e^{-\lambda|t-t'|}.$$

For the droplet's dynamics this value of Δ can be approximated by $\Delta \approx u/\kappa$ where $u = \sqrt{\beta/2 - 1}$ is the steady walking speed for the sinusoidal wave form. For the Langevin equation described in Eq. (28) with a dichotomous noise term, the exact solution for the stationary probability distribution of the variable q is [57]

$$P_{st}(q) = N(\Delta^2 - \gamma^2 q^2)^{\lambda/2\gamma - 1}, \quad (30)$$

where

$$N = \frac{\gamma \Gamma(1/2 + \lambda/2\gamma)}{\Delta^{\lambda/\gamma - 1} \Gamma(1/2) \Gamma(\lambda/2\gamma)}. \quad (31)$$

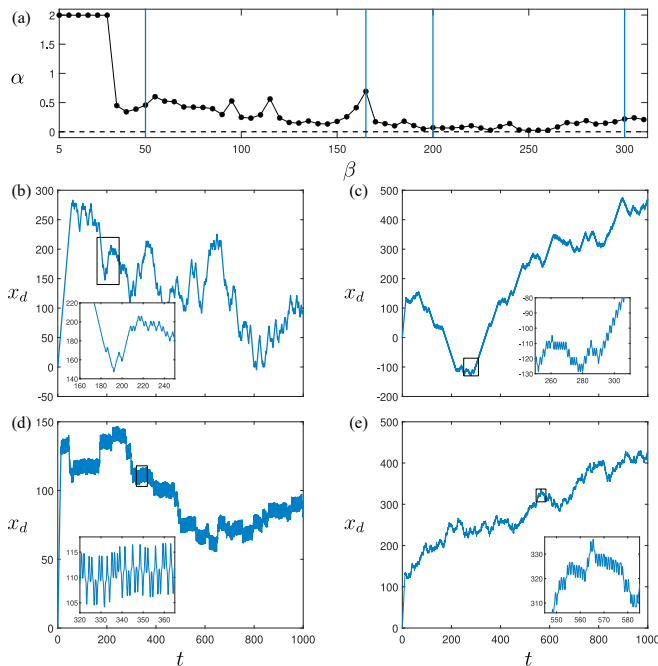


FIG. 12. Diffusion-like motion of the droplet for the sinusoidal wave form. (a) Diffusive exponent α as a function of the parameter β for a fixed $\kappa = 0.2$. Typical trajectories at (b) $\beta = 50$, (c) $\beta = 165$, (d) $\beta = 200$, and (e) $\beta = 300$ are shown. We calculate the diffusion exponent α from an ensemble of 1000 trajectories with each trajectory run for $t = 1000$.

The corresponding autocorrelation function is

$$\langle q(t)q(t') \rangle = \frac{-\lambda\Delta^2}{\gamma(\gamma^2 - \lambda^2)} e^{-\gamma(t-t')} + \frac{\Delta^2}{\gamma^2 - \lambda^2} e^{-\lambda(t-t')}. \quad (32)$$

A comparison of the Langevin model results with the numerical results for the stationary probability distribution of droplet's velocity and the velocity autocorrelation function is shown in Figs. 11(a) and (b) respectively. We find that the Langevin model captures the qualitative features of both of these plots.

C. Analysis of the diffusion-like dynamics

In 1828, Robert Brown observed the erratic motion of small particles suspended in water [58, 59]. We now know this as Brownian motion. Brownian motion plays a key role in modeling many random behaviors in nature and is typically modeled by considering random impulsive forces acting on particles. However, numerous investigations have shown the existence of Brownian-like motion from deterministic dynamics (also known as deterministic diffusion) in both discrete and continuous systems (see [48, 60–64] and the reference therein). In particular, deterministic diffusion have been shown in differential delay equations [48, 65].

By investigating the trajectories in the random walk-

like regime of the droplet with a sinusoidal wave field, we also obtain diffusion-like behavior for the droplet. The diffusive behavior of a system can be characterized by calculating how the mean squared displacement (MSD) scales with time, i.e., $\text{MSD} \sim t^\alpha$ with α being the diffusion exponent. If $\alpha = 2$ then the motion is ballistic while diffusive motion has $0 < \alpha < 2$ with $0 < \alpha < 1$ indicating sub-diffusive behavior, $\alpha = 1$ indicating diffusive motion and $1 < \alpha < 2$ indicating super-diffusive behavior. We plot the diffusion exponent α as a function of the parameter β for a fixed κ as shown in Fig. 12(a). We observe ballistic motion in the steady regime, while in the irregular walking regime, the diffusive exponent drops below 1, indicating that the motion is sub-diffusive. Some typical trajectories in the random walk-like regime are shown in Figs. 12(b)-(e).

We also note that as previously described in Eq. (21), the Lorenz system can be written as an integro-differential equation that describes a particle in a double-well potential. If in this equation the double-well potential is replaced by a periodic potential, then diffusive-like behavior in the variable X is observed [48] that is similar to what we see for the droplet's position x_d in Figs. 12 (a-d).

VIII. DISCUSSION AND CONCLUSION

We have explored the dynamics of a particle-wave entity in the (κ, β) parameter space using the stroboscopic model of Oza *et al.* [39] with different wave forms. We find that the steady walking state is always stable for a Gaussian wave form above the walking threshold, while for both the Bessel and the sinusoidal wave form, the steady walking becomes unstable for large β and small κ . By choosing a sinusoidal wave form with a Gaussian envelope and varying the length scale of spatial decay, we find that the instability region diminishes as the spatial decay is enhanced, suggesting that oscillations in the wave form are an essential dynamic feature for the instability of the steady walking motion. Moreover, the presence of even small spatial decay in the wave form results in the revival of the steady walking state for very large β . In the unsteady regime for the Bessel wave form and the sinusoidal wave form, we uncover a variety of unsteady motions such as oscillating walkers, self-trapped oscillations and irregular walkers. The oscillating walkers and self-trapped oscillations span an extended region in the parameter space for a sinusoidal wave form, while the presence of spatial decay in the Bessel wave form severely contracts the region spanned by both oscillating walkers and self-trapped oscillations.

Investigation of the irregular walking regime reveals that the projected chaotic attractor in the (v_d, \dot{v}_d) space has a striking resemblance to the Lorenz attractor, with the corresponding 1D return maps showing a similar cusp structure. In fact for the sinusoidal wave form, we find a one-to-one correspondence between the droplet's velocity

v_d and the dependent variable X in the Lorenz system. Durey [53] also explored bifurcations of the droplet's dynamics using established properties of the Lorenz system and identified several pilot-wave phenomena. This suggests a deeper connection between the dynamical system underlying walkers and the Lorenz system, and warrants further investigation. We also investigated the cusp map for the sinusoidal wave field and identified the different structures in the map with the corresponding physical dynamics of the droplet.

On exploring the statistical aspects of the time series for the droplet's velocity in the irregular walking regime, we find that in certain regions of the parameter space, the statistics of the reversals in the walking direction can be well approximated by a Markovian process. Moreover, by using the Langevin equation with dichotomous noise, we are able to capture the qualitative aspects of the stationary velocity distribution as well as the velocity autocorrelation function in the droplet's dynamics.

In summary, we have made explicit connections of the walking-droplet system to the Lorenz equations, the Langevin equation and deterministic diffusion. In future, it would be interesting to investigate the unsteady droplet dynamics in the (κ, β) parameter space using a stroboscopic model that allows the droplet to move in two spatial dimensions. The extra dimension may reveal novel unsteady regimes and alter the diffusive properties of the droplet dynamics.

ACKNOWLEDGMENTS

We thank Andy Hammerlindl for useful discussions. We acknowledge financial support from an Australian Government Research Training Program (RTP) Scholarship (R.V.) and the Australian Research Council via the Future Fellowship Project No. FT180100020 (T.S.).

Appendix A: Numerical simulations with the Bessel wave form

We numerically integrate Eq. (1) with the Bessel wave form using a modified version of the implicit Euler method. The second-order integro-differential equation in (1) can be rewritten as

$$\dot{x}_d = v_d, \quad (\text{A1})$$

and

$$\dot{v}_d = \frac{1}{\kappa} \left[\beta \int_{-\infty}^t J_1(x_d(t) - x_d(s)) e^{-(t-s)} ds - v_d \right]. \quad (\text{A2})$$

We assume the droplet is in the steady walking state with velocity u for $t \leq 0$. Discretizing Eqs. (A1) and (A2) using an explicit and an implicit Euler step respectively, results in

$$x_d(t_{i+1}) = x_d(t_i) + \Delta t v_d(t_i) \quad (\text{A3})$$

and

$$v_d(t_{i+1}) = \frac{1}{1 + \Delta t/\kappa} \left[v_d(t_i) + \frac{\Delta t \beta}{\kappa} \left(I(t_{i+1}) + \int_0^t J_1(x_d(t_{i+1}) - x_d(s)) e^{-(t_{i+1}-s)} ds \right) \right], \quad (\text{A4})$$

where the integral due to the initial condition $I(t_{i+1})$ is given by

$$I(t_{i+1}) = \int_{-\infty}^0 J_1(u(t_{i+1} - s)) e^{-(t_{i+1}-s)} ds. \quad (\text{A5})$$

The dimensionless time step was fixed at $\Delta t = 2^{-6}$. The integral in Eq. (A3) was performed using the MATLAB trapezoid function where we considered the contribution from all the previous impacts for the first 1280 timesteps ($t = 20$ using $\Delta t = 2^{-6}$) and then the contribution from the last 1280 impacts for $t > 20$. At 1280 previous impacts, the exponential time damping factor reached $e^{-20} \approx 10^{-9}$ so we neglected all contribution from impacts beyond 1280 previous steps. We used an implicit step for the velocity equation because the unsteady motion of the droplet arises in the region of parameter space with very small κ and very large β , where the integro-differential equation describing droplet motion becomes stiff. The initial-condition integral $I(t_{i+1})$ was performed using the MATLAB 'integral' function that uses global adaptive quadrature.

Appendix B: Numerical simulations with the sinusoidal wave form

To simulate the droplet's dynamics for a sinusoidal wave field, we can simplify the equation of motion by changing the integro-differential equation into a finite system of ordinary differential equations (ODEs). Substituting the sinusoidal wave form in Eq. (1) and using the addition formula for sine, we obtain

$$\kappa \ddot{x}_d + \dot{x}_d = \frac{\beta}{2} \left[\sin(x_d(t)) \int_{-\infty}^t \cos(x_d(s)) e^{-(t-s)} ds - \cos(x_d(t)) \int_{-\infty}^t \sin(x_d(s)) e^{-(t-s)} ds \right].$$

We define $y(t) = \int_{-\infty}^t \cos(x_d(s)) e^{-(t-s)} ds$ and $z(t) = \int_{-\infty}^t \sin(x_d(s)) e^{-(t-s)} ds$. These auxiliary variables satisfy

$$\dot{y} + y = \cos(x_d(t))$$

and

$$\dot{z} + z = \sin(x_d(t)).$$

Further letting $\dot{x}_d = v_d$, we obtain the system of ODEs

$$\dot{x}_d = v_d, \quad (\text{B1})$$

$$\kappa \dot{v}_d + v_d = \frac{1}{2}\beta [y \sin(x_d) - z \cos(x_d)], \quad (\text{B2})$$

$$\dot{y} + y = \cos(x_d), \quad (\text{B3})$$

$$\dot{z} + z = \sin(x_d). \quad (\text{B4})$$

We solve the system of Eqs. (B1) in MATLAB using the inbuilt ode45 solver. We initialized the simulations with the droplet in the steady walking state for t_{leg0} , which results in the following initial conditions for the system of ODEs: $x_d(0) = 0$, $v_d(0) = u$, $y(0) = 1/1 + u^2$ and $z(0) = -u/1 + u^2$. The simulations were run for a time $t = 1000$.

-
- [1] Y. Couder, E. Fort, C.-H. Gautier, and A. Boudaoud, From bouncing to floating: noncoalescence of drops on a fluid bath, *Phys. Rev. Lett.* **94**, 177801 (2005).
- [2] Y. Couder, S. Protière, E. Fort, and A. Boudaoud, Dynamical phenomena: Walking and orbiting droplets, *Nature* **437**, 208 (2005).
- [3] J. Moláček and J. W. M. Bush, Drops walking on a vibrating bath: towards a hydrodynamic pilot-wave theory, *J. Fluid Mech.* **727**, 612 (2013).
- [4] R. N. Valani, A. C. Slim, and T. Simula, Superwalking droplets, *Phys. Rev. Lett.* **123**, 024503 (2019).
- [5] M. Faraday, On a Peculiar Class of Acoustical Figures; and on Certain Forms Assumed by Groups of Particles upon Vibrating Elastic Surfaces, *Phil. Trans. Roy. Soc. London Series I* **121**, 299 (1831).
- [6] E. Fort, A. Eddi, A. Boudaoud, J. Moukhtar, and Y. Couder, Path-memory induced quantization of classical orbits, *Proc. Natl. Acad. Sci.* **107**, 17515 (2010).
- [7] D. M. Harris and J. W. M. Bush, Droplets walking in a rotating frame: from quantized orbits to multimodal statistics, *J. Fluid Mech.* **739**, 444–464 (2014).
- [8] A. U. Oza, D. M. Harris, R. R. Rosales, and J. W. M. Bush, Pilot-wave dynamics in a rotating frame: on the emergence of orbital quantization, *J. Fluid Mech.* **744**, 404 (2014).
- [9] S. Perrard, M. Labousse, E. Fort, and Y. Couder, Chaos driven by interfering memory, *Phys. Rev. Lett.* **113**, 104101 (2014).
- [10] S. Perrard, M. Labousse, M. Miskin, E. Fort, and Y. Couder, Self-organization into quantized eigenstates of a classical wave-driven particle, *Nat. Commun.* **5**, 3219 (2014).
- [11] M. Labousse, S. Perrard, Y. Couder, and E. Fort, Self-attraction into spinning eigenstates of a mobile wave source by its emission back-reaction, *Phys. Rev. E* **94**, 042224 (2016).
- [12] A. Eddi, J. Moukhtar, S. Perrard, E. Fort, and Y. Couder, Level splitting at macroscopic scale, *Phys. Rev. Lett.* **108**, 264503 (2012).
- [13] A. U. Oza, R. R. Rosales, and J. W. M. Bush, Hydrodynamic spin states, *Chaos* **28**, 096106 (2018).
- [14] D. M. Harris, J. Moukhtar, E. Fort, Y. Couder, and J. W. M. Bush, Wavelike statistics from pilot-wave dynamics in a circular corral, *Phys. Rev. E* **88**, 011001 (2013).
- [15] T. Gilet, Quantumlike statistics of deterministic wave-particle interactions in a circular cavity, *Phys. Rev. E* **93**, 042202 (2016).
- [16] P. J. Sáenz, T. Cristea-Platon, and J. W. M. Bush, Statistical projection effects in a hydrodynamic pilot-wave system, *Nat. Phys.* **14**, 315 (2018).
- [17] T. Cristea-Platon, P. J. Sáenz, and J. W. M. Bush, Walking droplets in a circular corral: Quantisation and chaos, *Chaos* **28**, 096116 (2018).
- [18] M. Durey, P. A. Milewski, and Z. Wang, Faraday pilot-wave dynamics in a circular corral, *J. Fluid Mech.* **891**, A3 (2020).
- [19] P. J. Sáenz, T. Cristea-Platon, and J. W. M. Bush, A hydrodynamic analog of Friedel oscillations, *Sci. Adv.* **6** (2020).
- [20] A. Eddi, E. Fort, F. Moisy, and Y. Couder, Unpredictable tunneling of a classical wave-particle association, *Phys. Rev. Lett.* **102**, 240401 (2009).
- [21] A. Nachbin, P. A. Milewski, and J. W. M. Bush, Tunneling with a hydrodynamic pilot-wave model, *Phys. Rev. Fluids* **2**, 034801 (2017).
- [22] L. Tadríst, T. Gilet, P. Schlagheck, and J. W. M. Bush, Predictability in a hydrodynamic pilot-wave system: Resolution of walker tunneling, *Phys. Rev. E* **102**, 013104 (2020).
- [23] R. N. Valani, A. C. Slim, and T. Simula, Hong–Ou–Mandel-like two-droplet correlations, *Chaos* **28**, 096104 (2018).
- [24] A. Nachbin, Walking droplets correlated at a distance, *Chaos* **28**, 096110 (2018).
- [25] Y. Dagan and J. W. M. Bush, Hydrodynamic quantum field theory: the free particle, *Comptes Rendus. Mécanique* **348**, 555 (2020).
- [26] M. Durey and J. W. M. Bush, Hydrodynamic quantum field theory: The onset of particle motion and the form of the pilot wave, *Front. Phys.* **8**, 300 (2020).
- [27] J. W. M. Bush, Pilot-wave hydrodynamics, *Annu. Rev. Fluid Mech.* **47**, 269 (2015).
- [28] J. W. M. Bush and A. U. Oza, Hydrodynamic quantum analogs, *Rep. Prog. Phys.* (2020).
- [29] S. E. Turton, M. M. P. Couchman, and J. W. M. Bush, A review of the theoretical modeling of walking droplets: Toward a generalized pilot-wave framework, *Chaos* **28**, 096111 (2018).
- [30] A. Rahman and D. Blackmore, Neimark-sacker bifurcations and evidence of chaos in a discrete dynamical model of walkers, *Chaos, Solitons & Fractals* **91**, 339 (2016).
- [31] R. N. Valani, J. Dring, T. P. Simula, and A. C. Slim, Emergence of superwalking droplets, *J. Fluid Mech.* **906**, A3 (2021).
- [32] V. Bacot, S. Perrard, M. Labousse, Y. Couder, and E. Fort, Multistable free states of an active particle from a coherent memory dynamics, *Phys. Rev. Lett.* **122**, 104303 (2019).
- [33] M. Hubert, S. Perrard, M. Labousse, N. Vandewalle, and Y. Couder, Tunable bimodal explorations of space from memory-driven deterministic dynamics, *Phys. Rev. E* **100**, 032201 (2019).

- [34] H. C. Berg and D. A. Brown, Chemotaxis in *Escherichia coli* analysed by three-dimensional tracking, *Nature* **239**, 500 (1972).
- [35] B. V. Hokmabad, R. Dey, M. Jalaal, D. Mohanty, M. Al-mukambetova, K. A. Baldwin, D. Lohse, and C. C. Maass, Emergence of bimodal motility in active droplets (2020), arXiv:2005.12721.
- [36] R. Stocker, Reverse and flick: Hybrid locomotion in bacteria, *Proc. Natl. Acad. Sci.* **108**, 2635 (2011).
- [37] T. Bhattacharjee and S. S. Datta, Bacterial hopping and trapping in porous media, *Nat. Commun.* **10**, 2075 (2019).
- [38] M. Durey, S. E. Turton, and J. W. M. Bush, Speed oscillations in classical pilot-wave dynamics, *Proc. Math. Phys. Eng. Sci.* **476**, 20190884 (2020).
- [39] A. U. Oza, R. R. Rosales, and J. W. M. Bush, A trajectory equation for walking droplets: hydrodynamic pilot-wave theory, *J. Fluid Mech.* **737**, 552 (2013).
- [40] R. N. Valani, *Superwalking Droplets and Generalised Pilot-Wave Dynamics*, Ph.D. thesis, Monash University (2020).
- [41] M. Durey, *Faraday wave-droplet dynamics: a hydrodynamic quantum analogue*, Ph.D. thesis, University of Bath (2018).
- [42] E. Fort and Y. Couder, Trajectory eigenmodes of an orbiting wave source, *Europhys. Lett.* **102**, 16005 (2013).
- [43] A. U. Oza, R. R. Rosales, and J. W. M. Bush, Hydrodynamic spin states, *Chaos* **28**, 096106 (2018).
- [44] C. Beck and F. Schögl, *Thermodynamics of Chaotic Systems: An Introduction*, Cambridge Nonlinear Science Series (Cambridge University Press, 1993).
- [45] C. Sparrow, *The Lorenz Equations: Bifurcations, Chaos, and Strange Attractors* (Springer-Verlag, New York, 1982).
- [46] E. N. Lorenz, Deterministic Nonperiodic Flow, *J Atmos Sci.* **20**, 130 (1963).
- [47] K. Takeyama, Dynamics of the Lorenz model of convective instabilities, *Prog. Theor. Phys.* **60**, 613 (1978).
- [48] R. Festa, A. Mazzino, and D. Vincenzi, Lorenz deterministic diffusion, *Europhys. Lett.* **60**, 820 (2002).
- [49] K. Takeyama, Dynamics of the Lorenz model of convective instabilities. II, *Prog. Theor. Phys.* **63**, 91 (1980).
- [50] R. Festa, A. Mazzino, and D. Vincenzi, Lorenz-like systems and classical dynamical equations with memory forcing: An alternate point of view for singling out the origin of chaos, *Phys. Rev. E* **65**, 046205 (2002).
- [51] H. M. Osinga and B. Krauskopf, Visualizing the structure of chaos in the Lorenz system, *Comput. Graph.* **26**, 815 (2002).
- [52] H. M. Osinga, Understanding the geometry of dynamics: the stable manifold of the Lorenz system, *J. R. Soc. N. Z.* **48**, 203 (2018).
- [53] M. Durey, Bifurcations and chaos in a Lorenz-like pilot-wave system, *Chaos* **30**, 103115 (2020).
- [54] R. M. Corless, Continued fractions and chaos, *Am. Math. Mon.* **99**, 203 (1992).
- [55] Y. Aizawa, Global aspects of the dissipative dynamical systems. I: Statistical identification and fractal properties of the Lorenz chaos, *Prog. Theor. Phys.* **68**, 64 (1982).
- [56] F. Aicardi and A. Borsellino, Statistical properties of flip-flop processes associated to the chaotic behavior of systems with strange attractors, *Biol. Cybern.* **55**, 377 (1987).
- [57] J. M. Sancho, Stochastic processes driven by dichotomous Markov noise: Some exact dynamical results, *J. Math. Phys.* **25**, 354 (1984).
- [58] R. Brown, XXVII. A brief account of microscopical observations made in the months of June, July and August 1827, on the particles contained in the pollen of plants; and on the general existence of active molecules in organic and inorganic bodies, *Philos. Mag.* **4**, 161 (1828).
- [59] R. Brown, XXIV. Additional remarks on active molecules, *Philos. Mag.* **6**, 161 (1829).
- [60] C. Beck, Dynamical systems of Langevin type, *Physica A* **233**, 419 (1996).
- [61] T. Shimizu, Chaotic force in Brownian motion, *Physica A* **195**, 113 (1993).
- [62] L. Chew and C. Ting, Microscopic chaos and Gaussian diffusion processes, *Physica A* **307**, 275 (2002).
- [63] G. Trefán, P. Grigolini, and B. J. West, Deterministic Brownian motion, *Phys. Rev. A* **45**, 1249 (1992).
- [64] G. Huerta-Cuellar, E. Jiménez-López, E. Campos-Cantón, and A. Pisarchik, An approach to generate deterministic Brownian motion, *Commun Nonlinear Sci Numer Simul* **19**, 2740 (2014).
- [65] J. Lei and M. C. Mackey, Deterministic Brownian motion generated from differential delay equations, *Phys. Rev. E* **84**, 041105 (2011).